Role of carbon and nitrogen in Fe_2C and Fe_2N from first-principles calculations

C. M. Fang,[1,2,*] M. A. van Huis,[2,3] J. Jansen,[2] and H. W. Zandbergen[2]

[1]*Materials Innovation Institute (M2i), 2628 CJ Delft, The Netherlands*

[2]*Kavli Institute of Nanoscience, Delft University of Technology, Lorentzweg 1, 2628 CJ Delft, The Netherlands*

[3]*Electron Microscopy for Materials Science, University of Antwerp, Groenenborgerlaan 171, 2020 Antwerp, Belgium*

(Received 1 June 2011; revised manuscript received 10 August 2011; published 8 September 2011)

Although Fe_2C and Fe_2N are technologically important materials, the exact nature of the chemical bonding of C and N atoms and the related impact on the electronic properties are at present unclear. Here, results of first-principles electronic structure calculations for Fe_2X (X = C, N) phases are presented. The electronic structure calculations show that the roles of N and C in iron nitrides and carbides are comparable, and that the X-X interactions have significant impact on electronic properties. Accurate analysis of the spatially resolved differences in electron densities reveals a subtle distinction between the chemical bonding and charge transfer of N and C ions.

DOI: 10.1103/PhysRevB.84.094102 PACS number(s): 61.66.Dk, 71.20.Be, 75.50.Bb, 31.10.+z

I. INTRODUCTION

The electronic and magnetic properties of Fe_2X (X = N and C) phases are of scientific interest and industrial importance for several reasons. First of all, Fe_2X (X = N and C) phases play an important role in steel-manufacturing processes and have strong impact on the properties of steels.[1–4] They are formed on the surfaces of iron in the processes of carburization and nitridation.[3–5] Second, these carbides and nitrides show interesting magnetic properties that are under investigation for potential applications.[1–3,5,6] Furthermore, Fe_2X carbides and nitrides exhibit multiple crystal structures (hexagonal ε-, orthorhombic ζ-, and η-forms), which have interesting mutual structural relationships.[2,7,8] Finally, knowledge about the role of carbon and nitrogen in Fe_2X carbides and nitrides is very useful to understand chemical reactions, such as nitridation and carburization of iron-related materials and the related effects on surface hardening and cracking mechanisms in steels.[1–5]

There have been many efforts by both experimentalists and theoreticians to understand the structural relationships[2,4,8–15] and the electronic and magnetic properties of Fe_2X carbides and nitrides as well as the differences between them.[2,8,16–24] Using x-ray diffraction (XRD), Jack investigated the crystal structures of the hexagonal ε-Fe_3X_{1+x} phases and their structural relationships with ζ-Fe_2N and η-Fe_2C.[10–12] Schwarz and coworkers performed high-pressure–high-temperature (HT-HP) experiments, revealing that orthorhombic ζ-Fe_2N transforms into the hexagonal ε-Fe_3X_{1+x} form at HT-HP conditions.[25] Using electron diffraction (ED), Nagakura and Tanehashi studied the electronic properties of ε-Fe_2N and ζ-Fe_2N phases and proposed different ionic models for ζ-Fe_2N and ε-Fe_2N.[2,8] Recently, Eck and coworkers investigated the electronic structures of iron nitrides, including ζ-Fe_2N.[5] Faraoun and coworkers studied the electronic structures of several iron carbides, including η-Fe_2C, using the full-potential linearized augmented plane wave (FP-LAPW) method.[17] Domain *et al*. studied the role of carbon and nitrogen atoms in ferrite (body-centered cubic (bcc) iron).[16] Boukhvalov and coworkers investigated the influence of interstitial C atoms on the electronic and magnetic properties of austenite (face-centered cubic (fcc) Fe).[26] Fang and coworkers performed first-principles calculations on the crystal-structural relationships between ε-Fe_2X (X = C, N) phases and the ζ- and η-forms.[20,21] Here, in order to understand the subtle differences in the interaction between Fe and X (X = C, N) atoms, a detailed comparison of the electronic properties of the ε-, ζ-, and η-phases of Fe_2X is presented. The insights into the roles of nitrogen and carbon in Fe_2X (X = C, N) phases are helpful for manipulation of physical properties, such as precipitation-induced hardness of steels.[1,27,28]

II. METHODS

The first-principle code VASP (Vienna *Ab initio* Simulation Program),[29,30] which employs density functional theory (DFT) within the Projector-Augmented Wave (PAW) method,[31,32] was used for all the calculations. The generalized gradient approximation (GGA) formulated by Perdew, Burke, and Ernzerhof (PBE) was employed for the exchange and correlation energy terms,[33] because the GGA describes spin-polarized Fe better than the local-density approximation (LDA).[34,35] The cutoff energy of the wave functions was 500 eV and 550 eV for carbides and nitrides, respectively. The cutoff energies of the augmentation functions were about 645 eV and 700 eV for carbides and nitrides, respectively. The electronic wave functions were sampled on a $16 \times 16 \times 24$ grid with 1053 k-points, a $16 \times 12 \times 16$ grid with 504 k-points, or a $12 \times 12 \times 16$ grid with 255 to 387 k-points, depending on the symmetry in the irreducible Brillouin zone (BZ) of η-Fe_2X, ζ-Fe_2X, and the supercell of ε-Fe_2X, respectively, using the Monkhorst and Pack method.[36] Structural optimizations were performed for both the lattice parameters and the relative atomic coordinates of atoms. The plane waves in the sphere were decomposed into C/N 2s, 2p, and 3d states, and Fe 4s, 4p, and 3d orbitals in the spheres for both spin-up (or majority) and spin-down (minority) electrons. In this way, a local magnetic moment was obtained from the difference of the spin-up electrons and spin-down electrons in the sphere. Tests of k-mesh and cutoff energies showed a good convergence (<1 meV/atom).

III. CALCULATED RESULTS

A. Structures and chemical bonds in Fe_2X phases

To have a measure of the relative stability of iron carbides/nitrides with respect to the elemental solids (α-Fe and

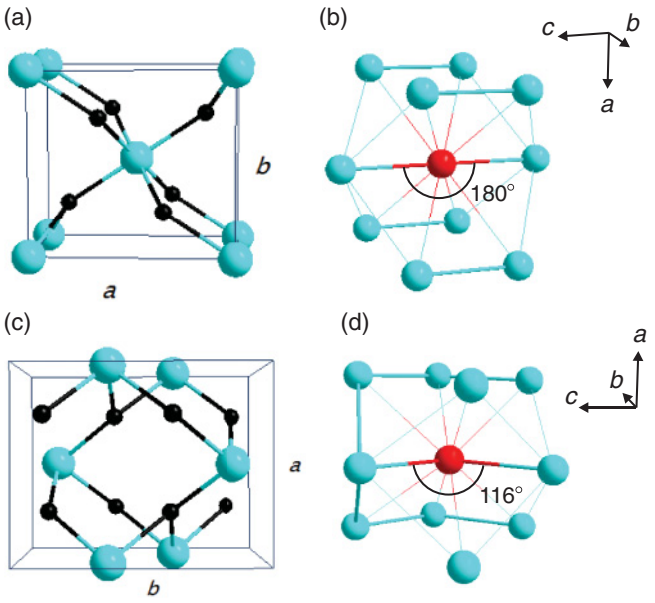

FIG. 1. (Color online) The schematic structures of η-Fe_2X (a) and ζ-Fe_2X (c), and (b, d) the X-X coordination. Thick lines represent short X-X bonds (about 2.85 Å), and thin lines represent long X-X bonds (about 3.48 Å) (Table II). The small solid black spheres represent Fe atoms; big green spheres represent X atoms. Note the straight X-X-X lines along the c-axis in η-Fe_2X, and the zigzag lines in ζ-Fe_2X.

graphite) and the N_2 molecule, the formation energy (ΔE_f) per atom of an iron carbide/nitride (Fe_2X) is employed, and defined as:

$$\Delta E_f = [E(Fe_2X) - (2\ H(Fe) + 1/2H(X_2))]/3. \quad (1)$$

At a temperature of 0 K and a pressure of 0 Pa, the enthalpy difference is equal to the energy difference, that is, $\Delta H(Fe_2X) = \Delta E(Fe_2X)$, when we ignore the zero-point vibration contribution.

The results of calculations for α-Fe and graphite were described in previous publications.[20,21,37,38] Calculations for nitrogen were performed in a cube with the axis length $a = 12.0$ Å, containing one N_2 molecule in order to avoid intermolecular interaction.[21] A cutoff energy for the wave functions of 1000 eV was employed to describe the strongly localized $2p$ bonds in the N_2 molecule. The calculated bond-length is 1.11 Å, which is in good agreement with the experimental value of 1.10 Å.

The structural relationships between Fe_2X phases, the ε-, η-, and ζ-forms, have been a subject of discussion for several decades.[2,3,6–16] Jack proposed that the crystal structure of η-Fe_2C originates from its ε-form *via* symmetry operations and a phase transformation from ε-Fe_2N to ζ-Fe_2N occurs *via* N rearrangements.[10–12] Careful analysis shows that Fe_2X phases have similar Fe-sublattices of hexagonally close-packed (hcp) structure with different occupations of the X atoms in the octahedral sites.[20,21] Figure 1(a) and 1(c) shows the schematic structures for η-Fe_2X and ζ-Fe_2X, respectively. At present, the widely used model for ε-Fe_2X has a supercell with dimensions $\sqrt{3}a_0 \times \sqrt{3}a_0 \times c_0$ (where a_0 and c_0 are the lattice parameters of a primitive hcp cell) with space group $P6_322$ (nr. 182).[2,8,10–12] This supercell contains 6 Fe atoms with two of the three X atoms at the 2c or 2d sites and the remaining X atom at one of the 2b sites.[2,11,12,18–21] Using a larger supercell with dimensions $2\sqrt{3}a_0 \times 2\sqrt{3}a_0 \times c_0$, ε-Fe_2X may have more configurations with different X arrangements. Table I lists the calculated results and the available experimental values in literature. Table II shows the calculated coordinates of atoms, chemical bonds, and local magnetic moments at the atomic sites.

Our calculated lattice parameters reproduced the experimental values as shown in Table I. As an example, the calculated lattice parameters of ζ-Fe_2N are $a = 4.3406$ Å, $b = 5.4480$ Å, $c = 4.7544$ Å, which are very close to the values ($a = 4.437$ Å, $b = 5.541$ Å, $c = 4.843$ Å) found by Rechnbach and Jacobs using neutron and high-resolution synchrotron diffraction at room temperature,[14] and to the values ($a = 4.425$ Å, $b = 5.523$ Å, $c = 4.830$ Å) obtained by Jack.[10–12]

TABLE I. The calculated results (lattice parameters [Å], formation energies ΔE [meV/atom], and magnetic moments M [μ_B per formula unit]) for Fe_2X phases using the DFT-GGA method. For the sake of comparison, the lengths of the a-axis of the supercell (see text) for ε-Fe_2X phases is reduced to half, $a^* = a_{Jack-3}/2$. The selected experimental values are in parentheses. The formation energy is $\Delta E = \{E[Fe_nX_m] - [n\ E(Fe) + m\ E(X)]\}/(n+m)$, where E(Fe) and E(X) are the calculated valence electron energies for the elemental solids, α-Fe and graphite, and gaseous N_2 molecules (details in Refs. 20 and 21).

Formula	Symmetry or X positions	Nitrides Latt. paras. (exp)	Nitrides $\Delta E/(M)$	Carbides Latt. paras. (Å) (exp)	Carbides $\Delta E/(M)$
ε–η phases					
ε-Fe_2X-a	X: 8c and	$a_\varepsilon* = 4.7474$ (4.794)[8]	−42.0/	$a^*_\varepsilon = 4.8025$(4.767)[8]	+35.3/
	4b in a plane	$c_\varepsilon = 4.4167$ (4.418)[8]	(2.94)	$c_\varepsilon = 4.2951$(4.353)[8]	(3.36)
η-Fe_2X	*Pnnm* (58)	$a_\eta = 4.7038$	−32.5/	$a_\eta = 4.7066$ (4.704)[8]	+17.4/
		$b_\eta = 4.3143$		$b_\eta = 4.2796$ (4.295)[8]	
		$c_\eta = 2.7686$	(2.87)	$c_\eta = 2.8242$ (2.830)[8]	(3.31)
ε–ζ phases					
ε-Fe_2X-c	X: 8c, 2b + 2b	$a^*_\varepsilon = 4.8672$ (4.794)[8]	−46.0/	$a^*_\varepsilon = 4.7991$(4.767)[8]	+27.9/
	in 2 planes	$c_\varepsilon = 4.3229$ (4.418) [8]	(2.90)	$c_\varepsilon = 4.2908$ (4.353)[8]	(3.35)
ζ-Fe_2X	*Pbcn* (60)	$a_\zeta = 4.3406$ (4.437)[13]	−46.1/	$a_\zeta = 4.2997$	+24.3/
		$b_\zeta = 5.4480$ (5.541)[13]	(2.98)	$b_\zeta = 5.4810$	(3.32)
		$c_\zeta = 4.7544$ (4.843)[13]		$c_\zeta = 4.8511$	

Table I also lists the calculated formation energies for Fe_2X (X = C, N) phases. All the iron-nitride phases are calculated to be stable relative to ferrite (α-Fe) and N_2 molecules, while all the carbide phases are meta-stable relative to the elemental solids (α-Fe and graphite). The forms η-Fe_2C and ζ-Fe_2N are more stable than the other phases of the same composition. This agrees with the fact that η-Fe_2N and ζ-Fe_2C structures have never been found experimentally.[2,10–12,19]

Table II lists the calculated atomic coordinates and the local magnetic moments in the atomic spheres for the η- and ζ-phases. As shown in Table II, the atomic coordination in the Fe_2X phases is similar, which is due to similar Fe-sublattices. Each Fe has 12 Fe neighbors and 3 X neighbors. Fe-Fe bonds are in the range between 2.67 and 2.77 Å in the η- and ζ-nitrides, while they are between 2.59 and 2.83 Å in carbides. The Fe-N bonds are in the range between 1.87 to 1.96 Å, which is larger than the Fe-C bonds (1.92 to 1.94 Å) in the carbides. Each C or N atom is positioned at the octahedral sites between the Fe atoms.

Table II and Fig. 1 also show that the N/C sublattices of the η-Fe_2X phases are less distorted than those of the ζ-phases. Each X atom has two X neighbors with short distances of 2.77 Å or 2.85 Å for nitrides and carbides, respectively. As shown in Fig. 1, the X-X-X bond angles are 180°, forming straight lines along the c-axis in the η-Fe_2X structures [Fig. 1(b)], while they are about 116 ° along the b-axis in the ζ-forms, forming zigzag lines [Fig. 1(d)]. The latter angles deviate slightly from the angles (120°) in ε-Fe_2X-c.

B. Electronic structures of Fe_2X phases

Figure 2 shows the calculated total density of states (tDOS) of these phases. Figure 3 shows the details of the partial density of states (pDOS) of atoms in η-Fe_2C and ζ-Fe_2N, as examples. Figure 4 shows the dispersion curves along the high-symmetry lines for the η-Fe_2X and ζ-Fe_2X phases.

As shown in Fig. 2, the electronic structures of Fe_2X (X = C, N) phases display similarities. The valence bands are composed of two separate parts. The Fermi level is at 0 eV for all the data in this present paper. At the lower energy range, the semicore C (N) 2s states form a broad band of about 3.1 eV (1.9 eV), ranging from −14.3 to −11.2 eV (from −18.3 eV to −16.4 eV). The shapes of the C (N) 2s bands are almost identical for both spin-up and spin-down electrons. Therefore, the C (N) 2s states do not contribute to the magnetism of these phases. The widths (about 3.1 eV) of the Fe_2C phases are larger than those of Fe_7C_3 (about 2.2 to 2.6 eV), of θ-Fe_3C (∼2.2 eV),[17,37,38] and of η-Fe_3C (∼2.5 eV).[18] The large widths of the C (N) 2s states indicate strong X-X interactions, as well as contributions to valence interactions, although they are semicore electrons. The larger dispersion of C 2s (band width ∼3.1 eV) in comparison to that of N 2s (∼1.9 eV) indicates that C ions in the carbides are more delocalized than N ions, in agreement with the fact that the radius of C^{4-} ions is 2.6 Å, which is much larger than that of N^{3-} ions (1.71 Å).[39]

There is an energy gap of about 3.3 eV (8.1 eV) between the C (N) 2s bands and the upper-energy bands, which are composed of mainly C (N) 2p and Fe 3d states, as shown in Fig. 4 for η-Fe_2C and ζ-Fe_2N. The lower part (from about −7.9 to −4.0 eV for carbides and from −8.3 to −4.5 eV for nitrides) of the X 2p–Fe 3d bands is dominated by C (N) 2p states, while the Fe 3d states are dominant in the upper part up to the Fermi level. The Fe 3d states are largely occupied for the spin-up electrons, while the Fermi level is at the middle of the Fe 3d states, as shown in Figs. 2 and 3. As shown Figs. 2 and 3, the shapes of the tDOSs show overall similarity between ε-Fe_2X-c and the ζ-forms, and between

TABLE II. The calculated coordinates, chemical bonds, and local magnetic moment M (μ_B/atom) in the atomic spheres.

Formula	Coordinates of atoms At. WP (x/a y/b z/c)	Bonds (Å)	M (μ_B)
η-Fe_2N	Fe 4g (0.6719, 0.2516, 0.0)	Fe-Fe: 2.67 (×4), 2.70 (×2),	+1.53
	N 2a (0.0, 0.0, 0.0)	2.73 (×4), 2.77 (×2)	
		-N: 1.89 (×2), 1.93	
		N-N: 2.77 (×2) (180°)	
		3.45 (×8)	−0.08
η-Fe_2C	Fe 4g (0.6554, 0.2499, 0.0)	Fe-Fe: 2.59 (×2), 2.71 (×4),	+1.71
	C 2a (0.0, 0.0, 0.0)	2.74 (×4), 2.82 (×2)	
		-C: 1.92 (×2), 1.94	
		C-C: 2.84 (×2) (180°)	−0.15
		3.48 (×8)	
ζ-Fe_2N	Fe 8d (0.2514, 0.1262, 0.0846)	Fe-Fe: 2.67, 2.68 (×2),	+1.56
	N 4c (0.0, 0.3646, $\frac{1}{4}$)	2.69 (×2), 2.71,	
		2.73 (×4), 2.75 (×2)	
		-N: 1.87, 1.92, 1.96	
		N-N: 2.85 (×2) (116.4°)	−0.07
		3.45 (×4), 3.48 (×4)	
ζ-Fe_2C	Fe 8d (0.2517, 0.1164, 0.0794)	Fe-Fe: 2.60, 2.63,	+1.70
	C 4c (0.0, 0.3636, $\frac{1}{4}$)	2.70, 2.71 (×2),	
		2.74 (×4), 2.83 (×2)	
		-C: 1.92 (×2), 1.93	
		C-C: 2.85 (×2) (116.7°)	−0.15
		3.47 (×4), 3.48 (×4)	

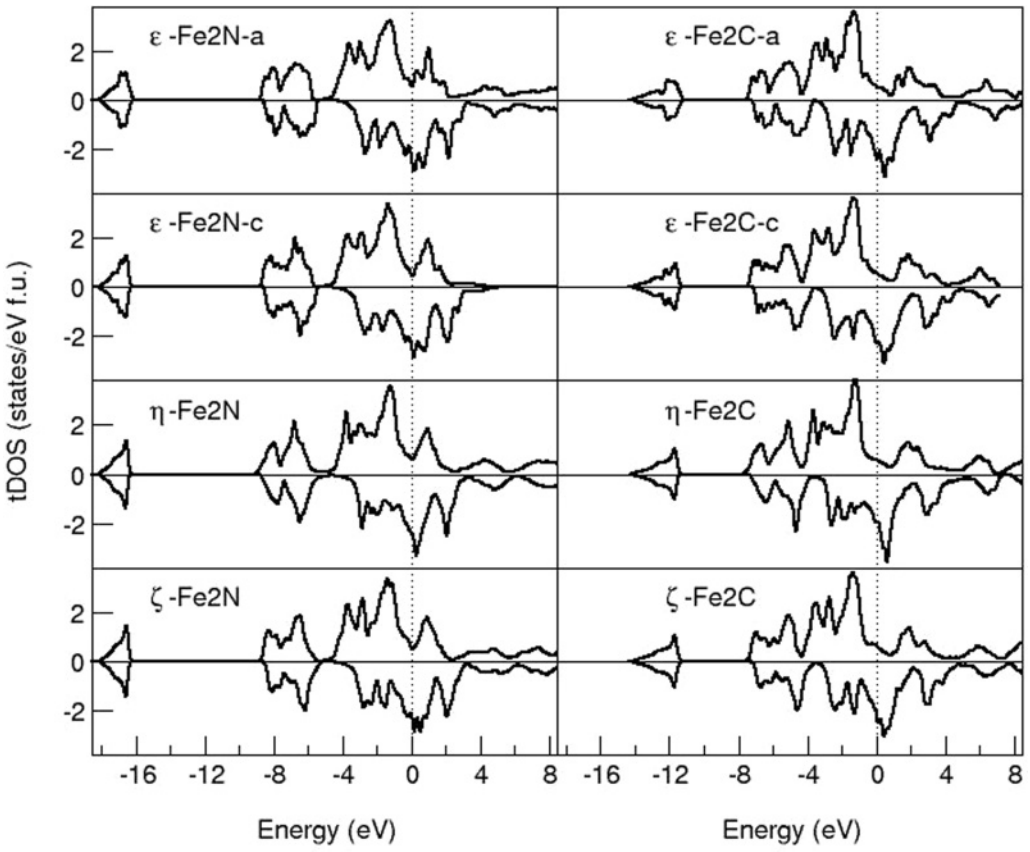

FIG. 2. Total density of states (tDOS) for the iron nitrides (left) and for the iron carbides (right). The negative values indicate the states for spin-down electrons, and positive values indicate the states for spin-up electrons.

ε-Fe_2X-a and the η-forms. This is due to the common hcp Fe sublattices in these phases. For spin-up (spin-down) electrons, there is a peak centered about +1 eV (+2 eV) above the Fermi level for nitrides and about +2 eV (+3 eV) above the Fermi level for carbides, respectively. These unoccupied states are dominated by Fe 3*d* and N/C 2*p* states, and they indicate that there are strong covalent features between C/N 2*p* and Fe 3*d* states. The exchange splitting due to spin polarization is about 2.0 eV for all the phases, which corresponds to the fact that the Fe sublattices in these carbides and nitrides are similarly hexagonal close-packed (hcp) structures. From Fig. 3, it is also apparent that the Fe *4s* and *4p* states are almost empty, except for some weak peaks mixing with the N/C 2*p* states, indicating that Fe *4s* electrons are transferred to the C/N sites.

Both the iron carbide and nitride were calculated to be ferromagnetic. As shown in Figs. 2 and 3, there are large differences for the DOSs at the Fermi level for the spin-up ($n_\uparrow[E_F]$) and spin-down ($n_\downarrow[E_F]$) electrons. For η-Fe_2C, $n_\uparrow(E_F) = 0.58$ states/eV per formula unit, and $n_\downarrow(E_F) = 1.93$ states/eV per formula unit. For ζ-Fe_2N, $n_\uparrow(E_F) = 0.55$ states/eV per formula unit, and $n_\downarrow(E_F) = 2.16$ states/eV per formula unit. Therefore, the spin-polarization $P = \{[n_\uparrow(E_F) - n_\downarrow(E_F)]/[n_\uparrow(E_F) + n_\downarrow(E_F)]\} = 54\%$ for η-Fe_2C, and $P = 57\%$ for ζ-Fe_2N. This indicates the potential for application of these materials in spintronics and magnetic recording media.[5,6]

Table I also lists the calculated magnetic moments integrated over the whole lattice. The Fe_2N phases have magnetic moments of about 2.9 μ_B/f.u. (formula unit), which are smaller than those (about 3.3 μ_B/f.u.) of the carbides. The calculations show a moment of 3.31 μ_B/f.u. for η-Fe_2C, which agrees with the previously calculated results (3.34 μ_B/f.u.) by Faraoun and coworkers.[17] Table II lists the calculated local moments in the atomic spheres ($R_{Fe} = 1.0$ Å and $R_N = 1.3$ Å). The Fe atoms have about 1.7 μ_B in the carbides and 1.5 μ_B in the nitrides. Both carbon and nitrogen atoms have magnetic moments antiparallel to that of iron. One nitrogen atom has a local moment of about −0.08 μ_B, which is smaller than that (about −0.15 μ_B) of a carbon atom (Table II). The calculated local magnetic moments for the nitrides agree with the recent calculations: 1.4 μ_B (Fe) and −0.06 μ_B (N) for ζ-Fe_2N.[24] Also, our calculated local magnetic moments (1.71 μ_B for Fe and −0.15 μ_B for C) for η-Fe_2C are close to those (1.66 μ_B for Fe and −0.12 μ_B for C) found by Faraoun and coworkers.[17]

To have a better understanding of the mixing between the N/C 2*p* and Fe 3*d* states, we show in Fig. 4 the dispersion curves close to the Fermi level along the high-symmetry lines in the Brillouin zone (BZ). The 6 C/N 2*p* bands in η-Fe_2X and 12 C/N 2*p* bands in ζ-Fe_2X can be well recognized when read in combination with Fig. 2. As shown in Fig. 4(g) and 4(h), it is remarkable that there are small gaps between the N 2*p* states and Fe 3*d* states in ζ-Fe_2N (at about −5 eV), while in η-Fe_2N, for the spin-up electrons, the N 2*p* bands and Fe 3*d* bands cross each other around the Γ point. As shown in Fig. 4(d), separation between the N 2*p* states and Fe 3*d* states

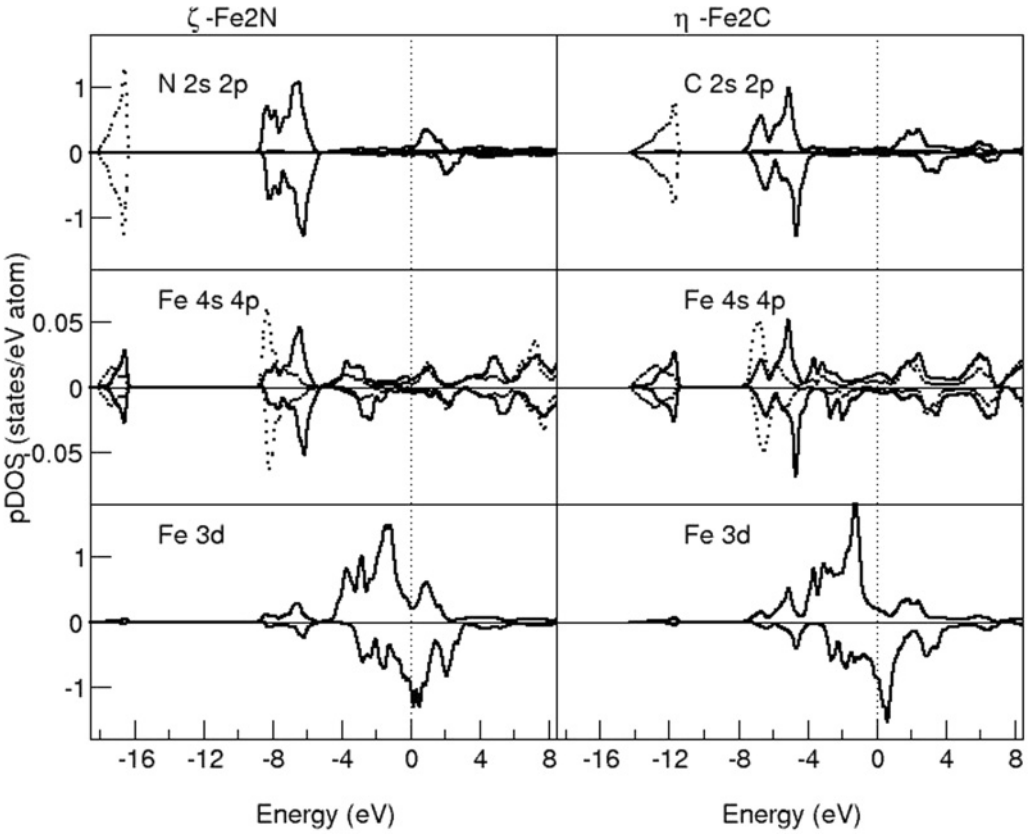

FIG. 3. Partial density of states (pDOS) of atoms in η-Fe_2C (left) and ζ-Fe_2N (right). The dotted lines represent the *s*-states. The meaning of negative (positive) signs is the same as in Fig. 2.

exists for the spin-down electrons in ζ-Fe_2C (at about -4 eV). This indicates that the role of C/N atoms in the compounds is not limited to being ionic, and that their arrangements have a strong impact on the electronic structure and chemical bonds. There are no apparent anisotropies in the band structure of all Fe_2X phases as shown in Fig. 4.

IV. DISCUSSION: THE ROLE OF C AND N IN Fe_2X PHASES

As shown in Figs. 2 and 3, the C/N 2*p* states are fully occupied. The Fe 4*s*, 4*p* states are almost empty. Therefore, at first approximation, the ionic model with formula $Fe^{2+}{}_2C^{4-}$ and $Fe^{1.5+}{}_2N^{3-}$ can be used to describe the chemical bonding in these carbides and nitrides, in agreement with the large differences between the electronegativity of the cations (C [2.55]/N [3.03]) and that of Fe (1.75).[39] The calculations also showed that for all the phases of iron nitride, the N atoms have similar chemical environments. Therefore, a different ionic model for the different phases of same chemical composition, $Fe^{1.5+}{}_2N^{3-}$ for ε-Fe_2N and $Fe^{0.75+}{}_2N^{1.5-}$ for ζ-Fe_2N, is very unlikely.[2,8] From the present calculations, it is also suggested for readers to be careful and alert about the ionic models for other transition-metal nitrides and carbides presented in literature.[2,8] Moreover, as shown in Figs. 2 and 3, there are also some unoccupied C/N 2*p* states above the Fermi level, which indicates a covalent character between C/N 2*p* and Fe 3*d* states.

We remark that all the valence electrons belong to the whole crystal rather than being localized to individual atoms/ions. That is clear from Figs. 2 and 3, where the C/N 2*s*, 2*p*, and Fe 3*d* states form bands with widths of 2 to 4 eV. We also note that there is no unique definition about the size of atoms/ions in solids, while the number of electrons integrated in the sphere of an atom strongly depends on its size. The Wigner-Seitz spheres for C/N employed here are considerably smaller than the usual ionic spheres for C^{4-} (R = 2.60 Å) and N^{3-} (R = 1.71 Å).[39] When the radius of Fe spheres is changed from $R_{sphere1}$ = 1.10 Å to $R_{sphere2}$ = 1.40 Å (volume change ratio V_2/V_1 = 2.062), the total number of electrons in the Fe spheres increases from about 6.20 to 7.80 electrons. When the ionic radii of N/C are changed from R_1 = 1.30 Å to R_2 = 1.00 Å (volume ratio V_2/V_1 = 0.455), the number electrons in the N spheres decreases from about 6.26 electrons to 4.60 electrons (difference of 1.66 electrons), while the number of electrons in C spheres decreases from 5.14 to 3.38 (difference of 1.76 electrons). Table III also shows that at the same size of spheres, there are about 0.1 to 0.2 electrons more in an N site than in a C site. That agrees with the more ionic character of N in comparison with C, as shown in Fig. 3.

Bader's charge analysis approach uniquely divides the atomic regions in a solid or molecule.[40,41] We performed calculations using the approach coded by Henkelman and coworkers.[42,43] The calculations give a charge transfer of about 0.57 e/Fe for the carbide and about 0.62 e/Fe for the nitride. There are no differences between the η- and ζ-structures. Therefore, the Bader charge analysis shows again the more ionic character of N in comparison to C.

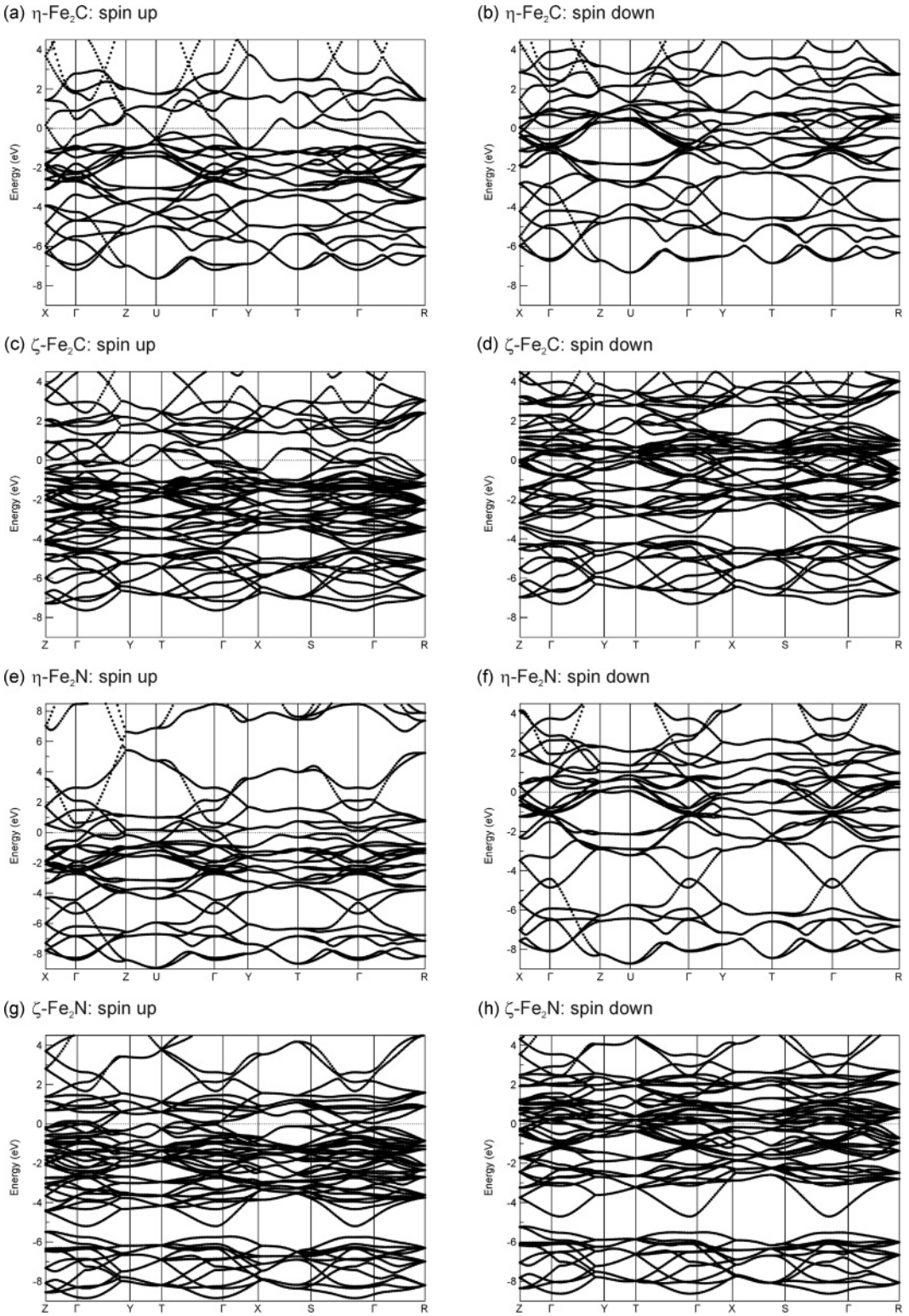

FIG. 4. Dispersion curves along the high-symmetry lines in the Brillouin zones (BZ) of η-Fe_2C (a, b), ζ-Fe_2C (c, d), η-Fe_2N (e, f), and ζ-Fe_2N (g, h).

Contour plots of electron density distributions, which do not depend on the choice of atomic radii, are very useful for detailed analysis of the chemical bonds and the charge transfer in a compound. We plotted the contours for both the carbides and nitrides in Fig. 5. The $z = 0.0$ and $z = 0.5$ planes are chosen because for η-Fe_2X, the Fe and X atoms are in the planes (Fig. 1).

There is strong similarity in the contour plots of the iron carbide (a, b) and iron nitride (c, d), particularly at the Fe sites (labeled by blue crosses), as shown in Fig. 5. The electron

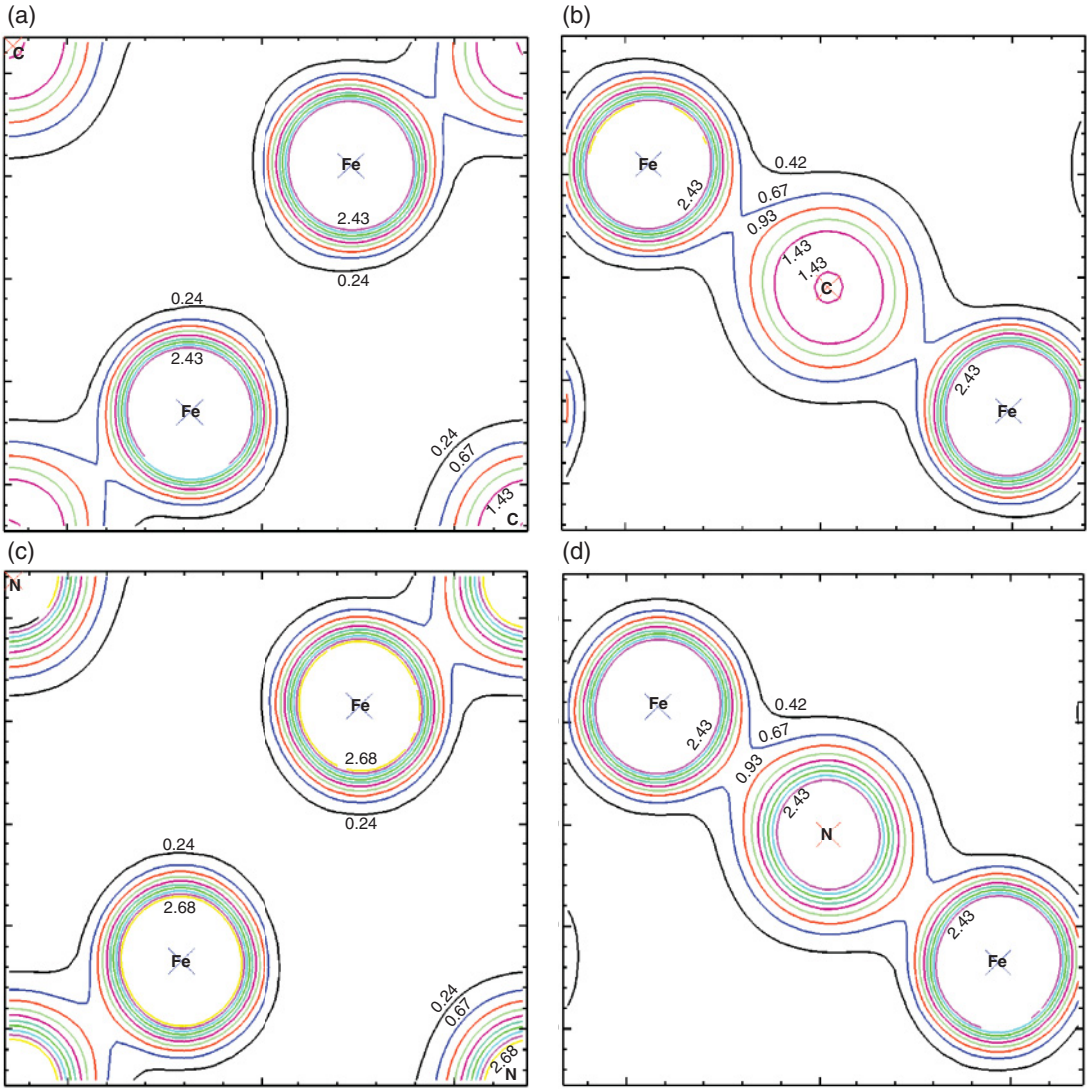

FIG. 5. (Color online) Contour plots for the electron densities, $\rho(x,y,z)$, of η-Fe_2C at $z = 0.0$ (a) and $z = 0.5$ (b), and of η-Fe_2N at $z = 0.0$ (c) and $z = 0.5$ (d). The contours are isocurves of constant electron density (electron/Å^3), as follows: ___0.42, ___0.67, ___0.93, ___1.18, ___1.43, ___1.68, ___1.93, ___2.18, ___2.43, ___2.68.

densities around the Fe sites and N/C sites are almost spherical. Overlaps occur between the electron densities of Fe and X. That indicates the chemical bonding between Fe and C/N. There are also some subtle differences. Clearly, the density at the C sites is much smaller than that at the N sites (Fig. 5). That is due to the fact that there is one more $2p$ electron at each N site than at the C site. Furthermore, the electron density between Fe-N is higher than that between Fe-C, indicating stronger Fe-N bonds. This corresponds to a larger charge transfer from Fe to N than from Fe to C (Table III). From these contour plots, the difference between iron carbides and nitrides is not clear due to the high absolute values.

Considering that the Fe_2X structures are composed of very similar Fe hcp sublattices with X as interstitial atoms, we made contour plots for the difference ($\Delta\rho_{Fe2X}[x,y,z]$) of electron densities for η-Fe_2X phases as follows. We first calculated the electron density distributions, $\rho_{Fe2X}(x,y,z)$ of η-Fe_2X (X = N, C). Using the same k-meshes and other computational settings, we then calculated separately the electron density distributions, $\rho_{Fe2}(x,y,z)$ of the Fe sublattices (removing N or C) and $\rho_X(x,y,z)$ of the N/C sublattices (removing Fe atoms). By subtracting the electron densities of the Fe sublattices and C/N sublattices from those of η-Fe_2X, the difference of the electron density distributions, $\Delta\rho_{Fe2X}(x,y,z)$, is obtained accordingly:

$$\Delta\rho_{Fe_2X}(x,y,z) = \rho_{Fe_2X}(x,y,z) - [\rho_{Fe_2}(x,y,z) + \rho_X(x,y,z)]. \quad (2)$$

Figure 6 shows the difference of electron densities ($\Delta\rho_{Fe2X}[x,y,z]$) for η-Fe_2C at $z = 0.0$ (a) and at $z = 0.5$ (b), as well as for η-Fe_2N at $z = 0.0$ (c) and at $z = 0.5$ (d). The black lines represent $\Delta\rho_{Fe2X}(x,y,z) = 0.0$, corresponding to zero charge transfer. The electrons are transferred from the areas with negative values to the areas with positive values in Fig. 6. In order to show the difference between C and N bonding in more detail, Fig. 7 shows line scans of $\Delta\rho_{Fe2X}(x,y,z)$ along the Fe-X-Fe lines (these are indicated with dash-dot

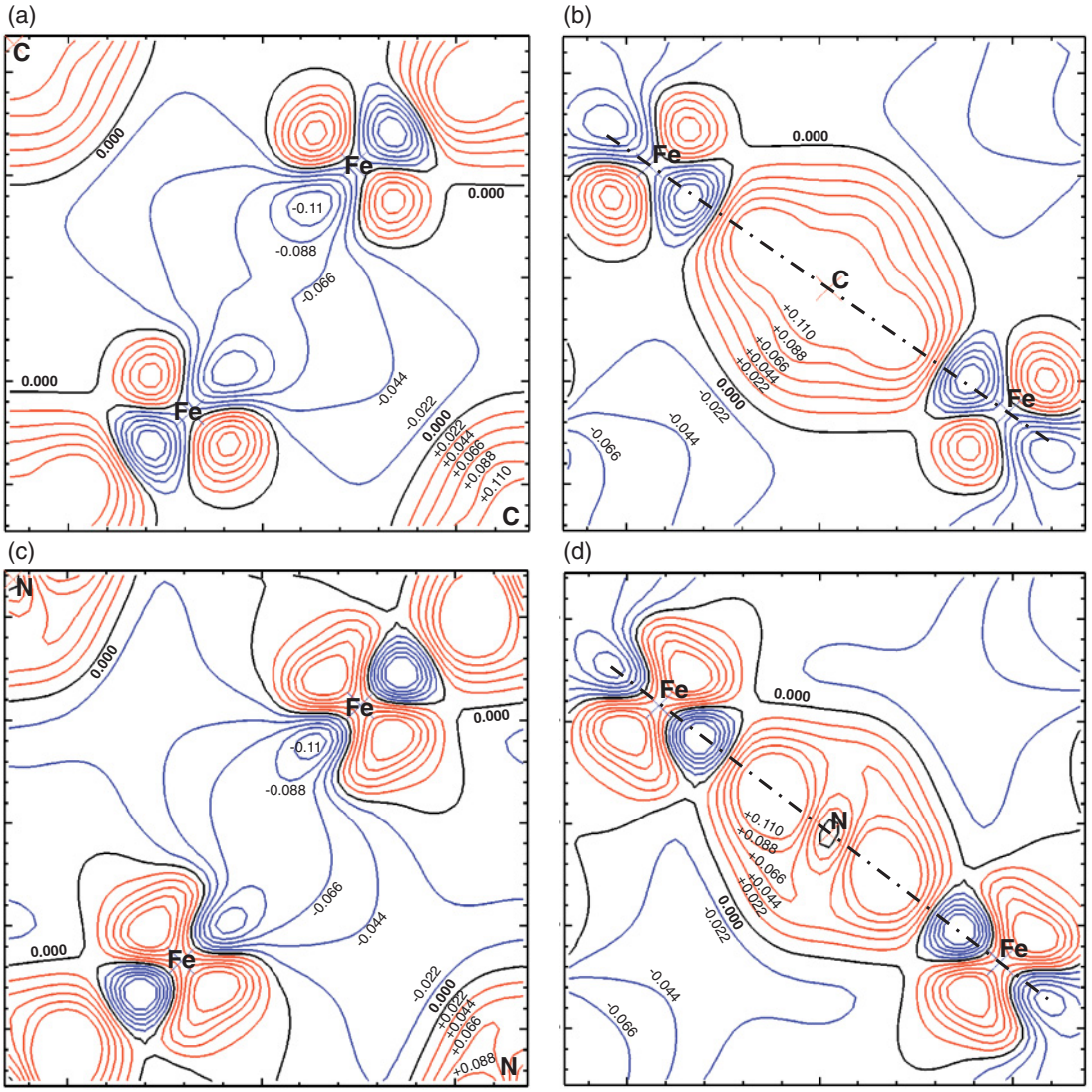

FIG. 6. (Color online) Contourplots displaying the difference in electron densities $\Delta\rho(x,y,z)$ as defined in Eq. (2) of the main text, for η-Fe_2C at $z = 0.0$ (a) and $z = 0.5$ (b), and for η-Fe_2N at $z = 0.0$ (c) and $z = 0.5$ (d). Strong similarity of the contour plots is apparent, but there are also distinct differences in the shape and magnitude of the electron densities between the carbide (a,b) and the nitride (c,d). The contours are isocurves of constant $\Delta\rho$ (electrons/Å^3). The solid black lines represent $\Delta\rho = 0.00$; the red/blue lines indicate positive/negative $\Delta\rho$ increasing/decreasing from zero (the black lines) by steps of $0.022/-0.022$. The dash-dot lines in (b) and (d) indicate the line scans along Fe-X-Fe that are shown in Fig. 7.

lines in Fig. 6(b) and 6(d)) for η-Fe_2X at $z = 0.5$. The $\Delta\rho$ values range from 0.0 e/Å^3 to ± 0.13 e/Å^3, which are much smaller than the values of the total electron density ρ (~ 2 e/Å^3), indicating that the net charge transfer is very subtle. Figure 6 reveals many common features for the nitrides and carbides:

(1) The areas around the C/N sites are negatively charged, in agreement with the larger electronegativities of C/N with respect to Fe.

(2) Around Fe, there are two distinct parts: Along the Fe-X-Fe line, the areas close to Fe are positively charged (negative sign in Fig. 6), while the areas perpendicular to the Fe-X-Fe lines are negatively charged (positive sign in Fig. 6). The most positively charged areas are between the Fe and X sites.

There are also distinct differences between the $\Delta\rho$ plots of the iron carbide and nitride.

(1) Around the X areas, the $\Delta\rho$ values of the carbide are higher than those of the nitride (Figs. 6 and 7), while the electron density at the N sites is much higher than that at the C sites (Fig. 5). This indicates that the N 2*s*, 2*p* electrons are more localized than those of carbon.

(2) As shown in Fig. 7, at the Fe sites, the electron-density difference is positive (negatively charged) for the nitride, while it is negative (positively charged) for the carbide. This is in agreement with the C^{-4} and N^{-3} ionic models (Table III).

(3) The contours in the Fe-Fe areas (blue cross) in Fig. 6 are similar for iron carbide and iron nitrides. However, along the X-Fe lines, the negative (positively charged) area between Fe-N atoms is small while $\Delta\rho$ is large in magnitude, in contrast to the same area between Fe-C atoms, where the negative area is larger but where $\Delta\rho$ is low in magnitude [Fig. 7]. That

TABLE III. Calculated electronic configurations and total electrons in the spheres of atoms in Fe_2X phases with different sizes of atomic spheres.

Formula	$R_{Fe} = 1.1$ Å, $R_X = 1.3$ Å Electronic config. (el.)	n(el.)	$R_{Fe} = 1.4$ Å, $R_X = 1.0$ Å Electronic config. (el.)	n(el.)
η-Fe_2N	Fe: $4s^{0.08}\ 4p^{0.11}\ 3d^{3.66}\uparrow$ $4s^{0.08}\ 4p^{0.11}\ 3d^{2.13}\downarrow$	6.18	Fe: $4s^{0.23}\ 4p^{0.35}\ 3d^{4.07}\uparrow$ $4s^{0.23}\ 4p^{0.36}\ 3d^{2.53}\downarrow$	7.76
	N: $2s^{0.88}\ 2p^{1.98}\ 3d^{0.22}\uparrow$ $2s^{0.88}\ 2p^{2.06}\ 3d^{0.21}\downarrow$	6.26	N: $2s^{0.73}\ 2p^{1.48}\ 3d^{0.05}\uparrow$ $2s^{0.73}\ 2p^{1.56}\ 3d^{0.05}\downarrow$	4.60
η-Fe_2C	Fe: $4s^{0.10}\ 4p^{0.12}\ 3d^{3.74}\uparrow$ $4s^{0.10}\ 4p^{0.12}\ 3d^{2.03}\downarrow$	6.20	Fe: $4s^{0.24}\ 4p^{0.36}\ 3d^{4.14}\uparrow$ $4s^{0.24}\ 4p^{0.38}\ 3d^{2.45}\downarrow$	7.81
	C: $2s^{0.77}\ 2p^{1.51}\ 3d^{0.21}\uparrow$ $2s^{0.78}\ 2p^{1.65}3d^{0.21}\downarrow$	5.13	C: $2s^{0.58}\ 2p^{1.00}\ 3d^{0.05}\uparrow$ $2s^{0.58}\ 2p^{1.12}\ 3d^{0.05}\downarrow$	3.38
ζ-Fe_2N	Fe: $4s^{0.08}\ 4p^{0.11}\ 3d^{3.67}\uparrow$ $4s^{0.08}\ 4p^{0.11}\ 3d^{2.11}\downarrow$	6.16	Fe: $4s^{0.23}\ 4p^{0.35}\ 3d^{4.09}\uparrow$ $4s^{0.23}\ 4p^{0.36}\ 3d^{2.51}\downarrow$	7.75
	N: $2s^{0.88}\ 2p^{1.99}\ 3d^{0.22}\uparrow$ $2s^{0.88}\ 2p^{2.07}\ 3d^{0.22}\downarrow$	6.26	N: $2s^{0.73}\ 2p^{1.62}\ 3d^{0.05}\uparrow$ $2s^{0.73}\ 2p^{1.55}\ 3d^{0.05}\downarrow$	4.60
ζ-Fe_2C	Fe: $4s^{0.10}\ 4p^{0.12}\ 3d^{3.73}\uparrow$ $4s^{0.09}\ 4p^{0.12}\ 3d^{2.03}\downarrow$	6.17	Fe: $4s^{0.24}\ 4p^{0.36}\ 3d^{4.15}\uparrow$ $4s^{0.24}\ 4p^{0.38}\ 3d^{2.44}\downarrow$	7.80
	C: $2s^{0.78}\ 2p^{1.51}\ 3d^{0.22}\uparrow$ $2s^{0.79}\ 2p^{1.66}\ 3d^{0.22}\downarrow$	5.15	C: $2s^{0.59}\ 2p^{1.00}\ 3d^{0.05}\uparrow$ $2s^{0.57}\ 2p^{1.12}\ 3d^{0.04}\downarrow$	3.37

indicates that the Fe-N bonding is more localized but stronger than the Fe-C bonding.

(4) The two positively charged areas near Fe and perpendicular to the Fe-X line are larger and have higher density differences for the nitride [Fig. 6(c) and 6(d)] than for the carbide [Fig. 6(a) and 6(b)]. That indicates larger charge transfer in the nitride than in the carbide.

From Figs. 6 and 7, it is clear that the features of the electron density difference $\Delta\rho$ are very subtle and strongly depend on the local crystal structure and coordination of atoms. The contour plots of $\Delta\rho_{Fe2X}(x,y,z)$ therefore provide much more detailed information in comparison with the integrated numbers of electrons in the atomic spheres, considering their dependency on the chosen sizes of atomic spheres (Table III).

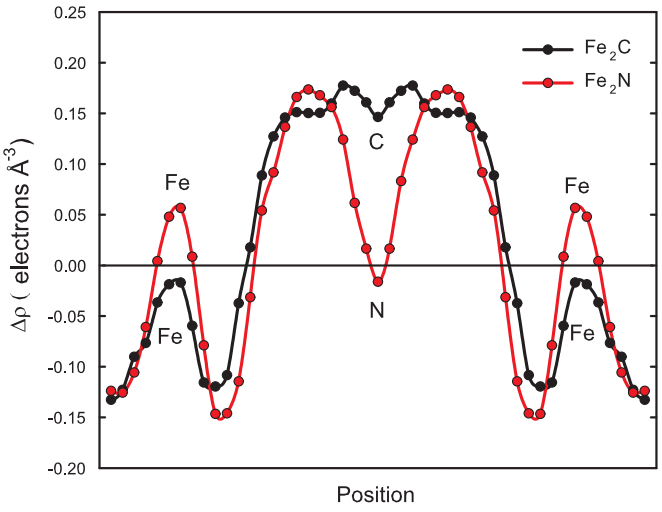

FIG. 7. (Color online) Line scans of the electron-density differences along the Fe-X-Fe lines (indicated in Fig. 6(a) and 6(b)) in the $z = 0.5$ plane for η-Fe_2N (black) and η-Fe_2C (red). The atom positions (Fe, C, N) are indicated. The black and red spheres represent the electron-density difference for η-Fe_2C and η-Fe_2N, respectively. Lines are drawn to guide the eyes.

V. CONCLUSIONS

The electronic band structure calculations showed that the overall shape of the Fe 3*d* states in the total DOS curves of Fe_2X (X = C, N) phases is very similar, corresponding to strong Fe 3*d*–Fe 3*d* metallic interactions. The (semicore) C/N 2*s* bands show a dispersed character, indicating strong X-X interactions. The wider band widths of C 2*s* in comparison to those of N 2*s* (3.1 eV vs 1.9 eV) show that the C ions are more delocalized than the N ions. All the C/N 2*s*, 2*p* states are almost fully occupied. The Fe-X interactions and charge transfer from Fe to C/N are clearly shown in the contour plots of the electron density distributions ($\rho_{Fe2X}[x,y,z]$), and in the difference of electron densities ($\Delta\rho_{Fe2X}[x,y,z]$). Therefore, the ionic models ($Fe^{2+}{}_2C^{4-}$, and $Fe^{1.5+}{}_2N^{3-}$) are valid as a first-order approximation. The present calculations also indicate that the different ionicity models, $(Fe^{+3/2})_2N^{-3}$ for ε-Fe_2N and $(Fe^{+3/4})_2N^{-3/2}$ for ζ-Fe_2N,[2,8] are rather inaccurate and are better not used when describing nitridization and carburization reactions. However, the ionic models are limited by the delocalized nature of the valence electrons and by the fact that charge transfer depends on the sphere sizes. Strong hybridization of C/N 2*p* with Fe 3*d* states indicates a covalent interaction between C/N 2*p* and Fe 3*d* states. Analysis of the electronic configurations in the atomic spheres, the dispersion curves, as well as the contour plots, shows that N is more ionic than C. Furthermore, detailed analysis of dispersion curves and electronic configurations suggests that N 2*s*, 2*p* states are more localized than those of C. Finally, all the Fe_2X phases are found to be ferromagnetic in the Fe sublattices, whereby the carbides have larger magnetic moments than the nitrides. The calculations also showed large spin-polarization effects.

ACKNOWLEDGMENTS

The authors acknowledge D. Hanlon (TATA-RDT) for kind help and discussions. We thank G. de Wijs (ESM, Radboud University) for his assistance with computational techniques and helpful discussions. The research was carried out under the Project Nos. MC5.06280 and MC.05239 in the framework of the Materials Innovation Institute (M2i; www.m2i.nl).

*c.fang@tudelft.nl, present address: Kavli Institute of Nanoscience, Delft University of Technology, Lorentzweg 1 NL 2628 CJ Delft, The Netherlands.

[1] K. H. Lo, C. H. Shek, and J. K. L. Lai, Mater. Sci. Eng. Rep. **65**, 39 (2009).
[2] S. Nagakura and S. Oketani, Trans. Iron Steel Inst. Jpn. **8**, 265 (1968).
[3] W. P. Tong, H. Zhang, J. Sun, L. Zuo, and J. C. He, J. Mater. Res. **25**, 2082 (2010).
[4] W. P. Tong, N. R. Ta, Z. B. Wang, J. Lu, and K. Lu, Science **299**, 686 (2003).
[5] B. Eck, R. Dronskowski, M. Takahashi, and S. Kikkawa, J. Mater. Chem. **9**, 1527 (1999).
[6] A. Leineweber, H. Jacobs, F. Hüning, H. Lueken, H. Schilder, and W. Kockelmann, J. Alloys Compd. **288**, 79 (1999).
[7] H. J. Goldschmidt, J. Iron Steel Inst. **160**, 345 (1948).
[8] S. Nagakuri and K. Tanehashi, J. Phys. Soc. Jpn. **25**, 840 (1968).
[9] G. Hägg, J. Iron Steel Inst. **130**, 439 (1934).
[10] K. J. Jack, Proc. R. Soc. London A **195**, 34 (1948).
[11] K. J. Jack, J. Iron Steel Inst. **169**, 26 (1951).
[12] K. J. Jack, Acta Cryst. **5**, 404 (1952).
[13] D. Rechenbach and H. Jacobs, J. Alloys Compd. **235**, 15 (1996).
[14] C. Middendorf and W. Mader, Z. Anorg. Allg. Chem. **627**, 398 (2001).
[15] C. Middendorf and W. Mader, Z. Metallkd. **94**, 333 (2003).
[16] C. Domain, C. S. Beequart, and J. Koct, Phys. Rev. B **69**, 144112 (2004).
[17] H. I. Faraoun, Y. D. Zhang, C. Esling, and H. Aourag, J. Appl. Phys. **99**, 093508 (2006).
[18] Z. Q. Lv, S. H. Sun, P. Jiang, B. Z. Wang, and W. T. Fu, Comput. Mater. Sci. **42**, 692 (2008).
[19] J. Jang, I. G. Kim, and H. K. D. H. Bhadeshia, Scr. Mater. **63**, 121 (2010).
[20] C. M. Fang, M. A. van Huis, and H. W. Zandbergen, Scr. Mater. **63**, 418 (2010).
[21] C. M. Fang, M. A. van Huis, and H. W. Zandbergen, Scr. Mater. **64**, 296 (2011).
[22] S. L. Shang, A. Böttger, and Z. K. Liu, Acta Mater. **56**, 719 (2008).
[23] S. L. Shang and A. Böttger, Acta Mater. **51**, 3597 (2003).
[24] M. Sifkovits, H. Smolinski, S. Hellwig, and W. Weber, J. Magn. Magn. Mater. **204**, 191 (1999).
[25] R. Niewa, D. Rau, A. Wosylus, K. Meier, M. Hanfland, M. Wessel, R. Dronskowski, D. A. Dzivenko, R. Riedel, and U. Schwarz, Chem. Mater. **21**, 391 (2009).
[26] D. W. Boukhvalov, Yu. N. Gornostyrev, M. I. Katsnelson, and A. I. Lichtenstein, Phys. Rev. Lett. **99**, 247205 (2007).
[27] J. W. Morris Jr., Science **320**, 1022 (2008).
[28] Y. Kimura, T. Inoue, F. X. Yin, and K. Tsuzaki, Science **320**, 1057 (2008).
[29] G. Kresse and J. Hafner, Phys. Rev. B **47**, 558 (1993).
[30] G. Kresse and J. Hafner, Phys. Rev. B **49**, 14251 (1994).
[31] P. E. Blöchl, Phys. Rev. B **50**, 17953 (1994).
[32] G. Kresse and J. Furthmüller, Phys. Rev. B **54**, 1758 (1999).
[33] J. P. Perdew, K. Burke, and M. Ernzerhof, Phys. Rev. Lett. **77**, 3865 (1996).
[34] C. Amador, W. R. Lambrecht, and B. Segall, Phys. Rev. B **46**, 1870 (1992).
[35] C. M. Fang, M. A. van Huis, M. H. F. Sluiter, and H. W. Zandbergen, Acta Mater. **58**, 2968 (2010).
[36] H. J. Monkhorst and J. D. Pack, Phys. Rev. B **13**, 5188 (1976).
[37] C. M. Fang, M.A. van Huis, and H. W. Zandbergen, Phys. Rev. B **80**, 224108 (2009).
[38] C. M. Fang, M. H. F. Sluiter, M. A. van Huis, C. K. Ande, and H. W. Zandbergen, Phys. Rev. Lett. **105**, 055503 (2010).
[39] *Handbook of Chemistry and Physics*, 90th ed. (CRC Press/Taylor and Francis, Boca Raton, FL, 2010), Sec. 9, p. 77.
[40] R. F. W. Bader, T. T. Nguyen-Dang, and Y. Tal, Rep. Prog. Phys. **44**, 893 (1981).
[41] R. F. W. Bader, J. Phys. Chem. A **102**, 7314 (1998).
[42] G. Henkelman, A. Arnaldsson, and H. Jónsson, Comput. Mater. Sci. **36**, 254 (2006).
[43] W. Tang, E. Sanville, and G. Henkelman, J. Phys. Condens. Matter **21**, 084204 (2009).